Available online at www.sciencedirect.com

ScienceDirect

Journal of Magnesium and Alloys 1 (2013) 201–209
www.elsevier.com/journals/journal-of-magnesium-and-alloys/2213-9567

Full length article

Electrochemical investigations on the corrosion behaviour of magnesium alloy ZE41 in a combined medium of chloride and sulphate

Nandini Dinodi, A. Nityananda Shetty*

Department of Chemistry, National Institute of Technology Karnataka, Surathkal, Srinivasnagar, Mangalore 575 025, Karnataka, India

Received 27 June 2013; accepted 21 August 2013

Abstract

The magnesium alloy ZE41 encompasses a wide spectrum of applications as a structural material. An extremely high susceptibility to corrosion limits widespread utility of ZE41. In the present study it has been attempted to understand the corrosion behaviour of ZE41 alloy employing electrochemical techniques like Tafel extrapolation and electrochemical impedance spectroscopy (EIS) in aqueous salt solutions containing mixture of sodium chloride and sodium sulphate over a varying range of electrolyte concentrations and solution temperatures. The morphology of the metal surface has been established by means of scanning electron microscopy (SEM). The results indicate that the rate of corrosion of ZE41 alloy increases with the increase in temperature and ionic concentration of the medium. The results of corrosion rates at varying temperatures have been utilized in the calculation of activation parameters such as activation energy, enthalpy of activation and entropy of activation for the corrosion process.

Keywords: Magnesium alloy; ZE41; EIS; SEM

1. Introduction

Magnesium is the lightest of all structural metals and majority of magnesium alloys are employed all over the world for weight-critical applications, owing to their high strength-to-weight ratio, low density, good damping characteristics, appreciably good castability, recyclability and excellent machinability [1–3]. Despite its natural abundance and plenty of advantages, application of magnesium and its alloys remains a limitation and a challenge, principally due to the poor corrosion resistance of these materials.

Several studies have established the corrosion behaviour of pure magnesium in variety of media, like chloride [4], sulphate [5,6] and engine coolants like ethylene glycol [7,8]. A lot of emphasis has been laid towards understanding the mechanism of anodic dissolution of magnesium in corrosive media [9,10]. A variety of magnesium alloys too have been extensively studied in order to establish the influence of the additive alloying elements and the microstructure on the corrosion behaviour of magnesium and its alloys [11–17]. Most popular among the magnesium alloys include those alloyed with Al and Mn (e.g. AM alloy series) and with Al, Zn and Mn (e.g. AZ alloy series). These alloys exhibit favourable properties for promising applications and their corrosion behaviour is well established [18–22]. However magnesium alloys containing rare earth elements continue to be the domain seldom explored, especially magnesium alloy ZE41 (Mg–Zn–Zr-RE). The addition of Zn is known to

* Corresponding author. Tel.: +91 824 2474200; fax: +91 824 2474033.
E-mail address: nityashreya@gmail.com (A. Nityananda Shetty).

Peer review under responsibility of National Engineering Research Center for Magnesium Alloys of China, Chongqing University

Production and hosting by Elsevier

http://dx.doi.org/10.1016/j.jma.2013.08.003

improve the mechanical strength of both cast and wrought alloys; Zr is added to refine the grain size and the addition of rare earth elements has been reported to improve the elevated temperature properties like creep performance [23]. With these combinations ZE41 alloy offers good strength, castability, creep resistance at a moderate cost, making it the perfect choice for selected applications.

Majority of ZE41 alloy parts find applications outdoor, where they get exposed to open atmosphere and often encounter aqueous salt environments (acid rain, salts in polluted humid air and road splash for automobile parts) which are potential corrosive media, triggering severe corrosion of the susceptible alloy. A thorough understanding the corrosion behaviour of the alloy in aqueous salt environment like aqueous chloride and sulphate solutions is a prerequisite in developing any corrosion controlling measure. A search of literature reveals that information available on electrochemical corrosion behaviour of ZE41 alloy in aqueous salt solutions is scarce. A few previous studies on ZE41 alloy have focused on establishing dry sliding wear behaviour [24], oxidation kinetics at high temperatures [25] as well as susceptibility to stress corrosion cracking [26] and micro-galvanic corrosion [27]. The influence of pH and chloride ion concentration on corrosion of ZE41 alloy was studied by Zhao [28]. However there seems to be no documented data describing the corrosion of ZE41 alloy in combined medium of sulphate and chloride. So the present study is intended to explore the corrosion behaviour of ZE41 alloy in a medium with chloride and sulphate ions, using electrochemical corrosion monitoring techniques.

2. Experimental part

2.1. Material

The specimen studied was magnesium alloy ZE41. The composition of the alloy sample is given in Table 1. The working electrode received as a rod was transformed into a cylindrical test coupon by embedding in epoxy resin, there by exposing a definite open surface area of 0.732 cm^2. This coupon was polished as per standard metallographic practice, belt grinding followed by polishing on emery papers of grade 600, 800, 1000, 1200, 1500, 2000, finally on polishing wheel using legated alumina abrasive to obtain mirror finish. The polished specimen was washed with double distilled water, degreased with acetone and dried before immersing in the sodium sulphate medium.

Table 1
Composition of specimen (% by weight).

Element	% Composition	Element	% Composition
Zn	4.59	Sn	<0.002
Ce	1.05	Pb	<0.002
Zr	0.7	Cu	<0.002
La	0.48	Be	<0.001
Pr	0.12	Ni	<0.001
Mn	0.02	Cr	<0.001
Nd	<0.01	Sr	<0.001
Fe	0.006	Mg	Balance
Al	0.004		

2.2. Medium

The electrolyte media of total six different concentrations 0.2 M Na_2SO_4−0.1 M NaCl, 0.2 M Na_2SO_4−1.0 M NaCl, 0.6 M Na_2SO_4−0.1 M NaCl, 0.6 M Na_2SO_4−1.0 M NaCl, 1.0 M Na_2SO_4−0.1 M NaCl and 1.0 M Na_2SO_4−1.0 M NaCl were prepared by dissolving appropriate amounts of, both analytical grade sodium sulphate and sodium chloride salts in double distilled water. The corrosion studies were carried out at temperatures 30 °C, 35 °C, 40 °C, 45 °C, 50 °C (±0.5 °C) in a calibrated thermostat.

2.3. Electrochemical measurements

Electrochemical measurements were carried out using electrochemical work station, Gill AC having ACM instrument Version 5 software. The arrangement employed was a conventional three-electrode Pyrex glass cell with a platinum counter electrode, a saturated calomel electrode (SCE) as reference and the ZE41 alloy specimen as the working electrode. All the values of potential reported are referred to the SCE. The polarization studies were carried out immediately after the EIS studies on the same exposed electrode surface without any additional surface treatment.

2.3.1. Potentiodynamic polarization studies

Well polished ZE41 alloy specimen coupon was exposed to the corrosion medium at different temperatures (30−50 °C) and allowed to establish a steady-state open circuit potentials (OCP). The potentiodynamic current−potential curves (Tafel curves) were recorded by polarizing the specimen to −250 mV cathodically and +250 mV anodically, relative to the OCP at a scan rate of 1 mV s^{-1}.

2.3.2. Electrochemical impedance spectroscopy (EIS) studies

Impedance measurements were performed at open circuit potential (OCP) by the application of a periodic small amplitude (10 mV) ac voltage signal with a wide spectrum of frequency ranging from 100 kHz to 0.01 Hz. The impedance data were analysed using Nyquist plots.

In all the above measurements, at least three similar results were considered and their average values have been reported.

2.4. Scanning electron microscopy (SEM) analysis

The surface morphology of the ZE41 specimen in the presence and absence of the corrosive medium were established by recording SEM images of the corresponding samples using JEOL JSM-6380LA analytical scanning electron microscope.

3. Results and discussion

3.1. Potentiodynamic polarization measurements

The polarization measurements of ZE41 alloy specimen were carried out in combined salt media of varying concentrations and at different solution temperatures using Tafel polarization method. Fig. 1 shows the potentiodynamic polarization curves for the corrosion of ZE41 alloy in 1.0 M Na_2SO_4, containing different concentrations of chloride ions at 30 °C. Fig. 2 shows the potentiodynamic polarization curves for the corrosion of ZE41 alloy 0.1 M NaCl, containing different concentrations of sulphate ions at 30 °C. As seen from the Figs. 1 and 2 the polarization curves are shifted to the higher current density region with the increase in chloride and sulphate concentration, indicating an increased rate of corrosion. Similar plots have been obtained at other conditions under consideration. The anodic polarization curves did not exhibit linear behaviour and are assumed to represent anodic oxidation of magnesium. The anodic branches showed the inflection points at potentials more positive than corrosion potential (E_{corr}), characterized by two different slopes indicating a kinetic barrier effect, possibly due to the deposition of a surface film followed by its dissolution at increased anodic potential. Similar observations have been reported earlier [22,28]. However, the cathodic branch of polarization curves showed linear behaviour and thought to represent cathodic hydrogen evolution through the reduction of water. The corrosion current density (i_{corr}) was deduced from the extrapolation of cathodic branch of the Tafel plots to the corrosion potential. The slopes of the Tafel branches change with the varying medium concentration, without any modifications in overall shape, which indicate that the strength of medium strongly influences kinetics of the cathodic hydrogen evolution and the anodic metal dissolution reactions without altering the mechanism of alloy corrosion.

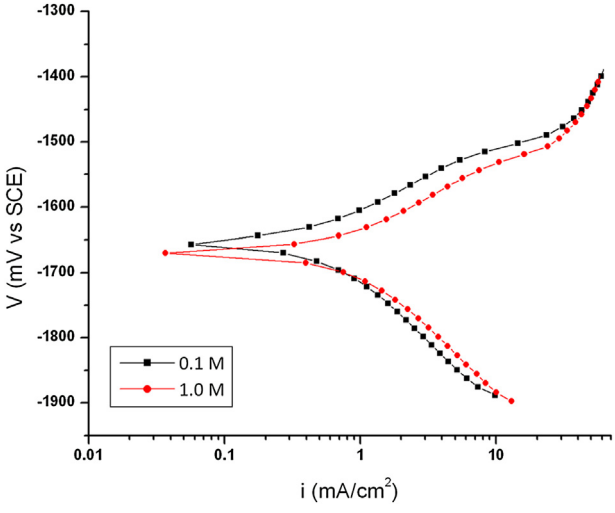

Fig. 1. Potentiodynamic polarization curves for the corrosion of ZE41 alloy in 1.0 M Na_2SO_4 in the presence of different concentrations of NaCl at 30 °C.

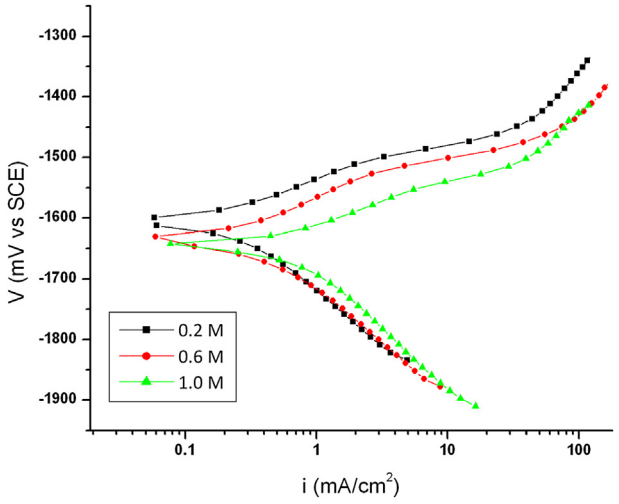

Fig. 2. Potentiodynamic polarization curves for the corrosion of ZE41 alloy in 0.1 M NaCl in the presence of different concentrations of Na_2SO_4 at 30 °C.

The potentiodynamic polarization parameters such as corrosion potential (E_{corr}), corrosion current density (i_{corr}), cathodic slope (b_c) were deduced from the Tafel plots and are tabulated in Table 2. The corrosion rate (υ_{corr}) was calculated using the following equation [29]:

$$\upsilon_{corr}(\text{mm/year}) = (K \times i_{corr} \times EW)/\rho \quad (1)$$

where, constant $K = 0.00327$ defines the unit of corrosion rate (mm y^{-1}), i_{corr} is the corrosion current density in μA cm^{-2}, ρ is the density of the corroding material, 1.84 g m^{-3}, EW is the equivalent weight of the alloy calculated using equation shown below:

$$EW = 1/\sum[(n_i \times f_i)/(W_i)] \quad (2)$$

where f_i is the weight fraction of the ith element in the alloy, W_i is the atomic weight of the ith element in the alloy and n_i is the valence of the ith element of the alloy [29].

It is evident from the data tabulated in Table 2 that a higher corrosion rate is associated with a higher sulphate concentration at each chloride concentration and vice versa, which reflects that the corrosive strength strongly influences rate of alloy corrosion. Even though sulphate is regarded as a mild corrosive compared to chloride, sulphate has been reported to possess an appreciable influence on the electrochemical behaviour of pure magnesium and some of its alloys [5,6,30]. The corrosiveness of these ions towards magnesium and its alloys arises from their tendency to cause surface film breakdown by the dissolution of the deposited corrosion product. The corrosion potential (E_{corr}), shifts towards more negative (more active) values with the increase in the rate of corrosion. Although this trend of a more negative E_{corr} associated with a higher corrosion rate had been observed by Baril and Pebere [6] for pure magnesium corrosion in sulphate medium and by Zhao [28] for corrosion of ZE41 alloy in chloride medium, this behaviour cannot be concluded as a

Table 2
Electrochemical polarization parameters for the corrosion of ZE41 alloy in different concentrations of Na_2SO_4 and NaCl, at different temperatures.

Na_2SO_4 concentration/mol dm^{-3}	NaCl concentration/mol dm^{-3}	Temperature/°C	E_{corr}/mV(SCE)	i_{corr}/μA cm^{-2}	$-b_c$/mV dec^{-1}	υ_{corr}/mm y^{-1}
0.2	0.1	30	−1607	242.87	176	5.41
		35	−1628	297.29	195	6.62
		40	−1644	364.85	196	8.12
		45	−1649	495.16	192	11.02
		50	−1655	914.10	213	20.35
0.2	1.0	30	−1642	449.86	195	10.02
		35	−1648	498.95	199	11.12
		40	−1654	556.85	202	12.39
		45	−1658	797.67	204	17.76
		50	−1667	1248.82	210	27.81
0.6	0.1	30	−1635	381.20	186	8.49
		35	−1635	692.98	203	15.43
		40	−1631	792.68	210	17.65
		45	−1657	955.02	190	21.26
		50	−1653	1302.60	226	29.01
0.6	1.0	30	−1644	641.30	198	14.28
		35	−1648	817.18	209	18.19
		40	−1657	913.02	213	20.33
		45	−1668	1229.20	217	27.37
		50	−1667	1541.20	218	34.31
1.0	0.1	30	−1654	554.74	202	12.25
		35	−1659	800.04	199	17.81
		40	−1663	1101.03	198	24.51
		45	−1696	1451.30	228	32.31
		50	−1697	1540.40	219	35.38
1.0	1.0	30	−1669	825.04	204	18.37
		35	−1681	1034.70	214	23.04
		40	−1665	1310.20	221	29.17
		45	−1716	1733.50	217	38.59
		50	−1726	1752.80	224	39.03

phenomenon, as in majority of studies no such direct relation between E_{corr} and corrosion rate had been reported.

In aqueous solutions the oxidation and corrosion of magnesium can be summarized by the following reactions [11]:

$$Mg \rightarrow Mg^{+} + e^{-} \quad (3)$$

$$Mg \rightarrow Mg^{2+} + 2e^{-} \quad (4)$$

The standard electrode potential of magnesium is −2.38 V, but the steady state working potential is about −1.5 V. The difference in potential has been attributed to the formation of $Mg(OH)_2$ film on the metal surface [31]. There are two oxidation processes involved in the anodic dissolution of magnesium and its alloys. At more active potentials around −2.78 V (vs SCE) magnesium is oxidized to monovalent magnesium ion and at slightly higher potentials of −1.56 V (vs SCE) oxidation to divalent magnesium ion takes place in parallel with the former oxidation [10]. Monovalent magnesium ion being unstable undergoes oxidation to divalent magnesium ion through a series of reactions involving unstable intermediates like magnesium hydride as shown in equations below:

$$Mg^{+} + 2H^{+} + 3e^{-} \rightarrow MgH_2 \quad (5)$$

$$MgH_2 + 2H_2O \rightarrow Mg^{2+} + 2OH^{-} + 2H_2 \quad (6)$$

$$Mg^{2+} + 2OH^{-} \rightarrow Mg(OH)_2 \quad (7)$$

$$2\,Mg^{+} + 2H_2O \rightarrow Mg^{2+} + Mg(OH)_2 + H_2 \quad (8)$$

The microstructure of ZE41 consists of the α-Mg matrix with second phase (β-phase) particles non-uniformly distributed

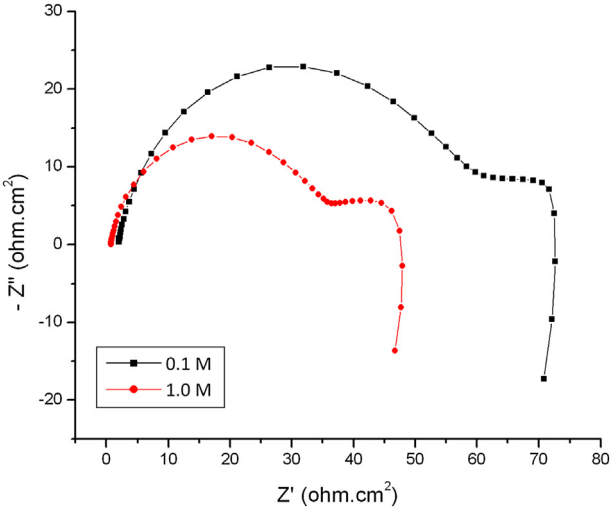

Fig. 3. Nyquist plots for the corrosion of ZE41 alloy in 0.6 M Na_2SO_4 in the presence of different concentrations of NaCl at 30 °C.

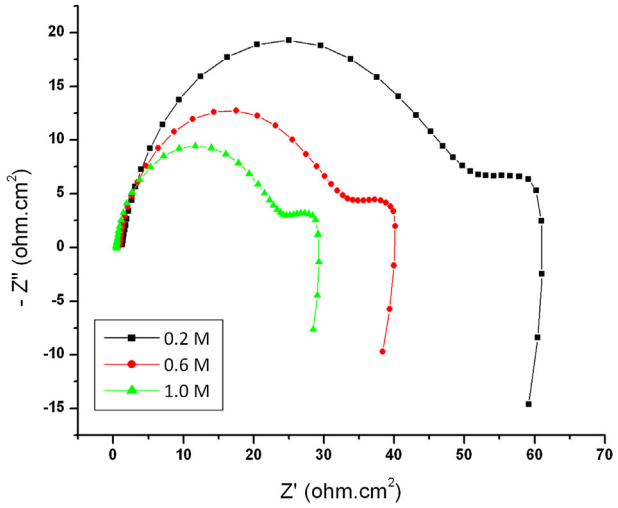

Fig. 4. Nyquist plots for the corrosion of ZE41 alloy in 0.1 M NaCl in the presence of different concentrations of Na_2SO_4 at 40 °C.

throughout and the T-phase distributed eutectically at the grain boundaries. The β-phase particles are rich in zirconium (Zr_4Zn) and T-phase comprises of rare earth elements (Mg_7Zn_3RE), the composition of these secondary phases have been reported earlier [27,28]. These secondary phases are cathodic to α-Mg matrix and hence ZE41 alloy undergoes severe micro-galvanic corrosion, where α-Mg matrix corrodes as anode and secondary phases are protected as cathodes [12−17,27]. The main corrosion product $Mg(OH)_2$ preferentially precipitates over the α-Mg matrix and the continuity of this surface film is interrupted by the presence of secondary phases, making the surface film inherently partially protective. In addition the secondary oxidation results in chemical liberation of hydrogen gas at the anode. The film breakdown at higher anodic overvoltage thus can be explained as the consequence of rapidly evolving hydrogen at anodic sites as hinted by the inflection in anodic branch of Tafel plots.

Nordlien [32] reported that the corrosion product film on the magnesium surface is multilayered, comprising of inner cellular layer of MgO−$Mg(OH)_2$, an intermediate thin film of MgO and an outer thick porous $Mg(OH)_2$ layer. Several studies have concluded the surface layer to be partially protective, with corrosion reactions occurring predominantly at the breaks and imperfections of the film [33−35]. The phenomenon of chemical evolution of hydrogen at anode and the partially protective surface film are the best explanations among the several mechanisms proposed to explain the strange anodic dissolution behaviour of magnesium referred to as Negative Difference Effect (NDE) [4].

3.2. Electrochemical impedance spectroscopy

The Nyquist plots for the corrosion of ZE41 alloy in 0.6 M Na_2SO_4 containing different concentrations of chloride ions are shown in Fig. 3 at 30 °C. Fig. 4 represents the Nyquist plots for

Table 3
Impedance parameters for the corrosion of ZE41 alloy in different concentrations of Na_2SO_4 and NaCl, at different temperatures.

Na_2SO_4 concentration/mol dm^{-3}	NaCl concentration/mol dm^{-3}	Temperature/°C	R_{ht}/Ω cm^2	R_f/Ω cm^2	C_{dl}/μF cm^{-2}	C_f/μF cm^{-2}
0.2	0.1	30	74.9	69.7	27.13	101.82
		35	54.6	49.0	36.42	103.61
		40	49.2	34.2	39.04	106.14
		45	43.2	31.8	43.06	107.72
		50	28.8	25.7	45.62	110.64
0.2	1.0	30	52.6	38.6	38.16	108.58
		35	46.0	26.9	48.27	109.62
		40	42.9	21.7	52.16	110.89
		45	34.6	20.1	56.38	112.08
		50	19.3	19.9	61.82	116.92
0.6	0.1	30	47.2	46.0	29.13	102.42
		35	38.1	30.1	37.02	104.94
		40	33.4	24.9	39.82	106.98
		45	25.9	17.9	44.20	109.28
		50	18.8	16.2	47.09	111.38
0.6	1.0	30	38.0	32.5	39.42	108.92
		35	26.3	26.0	48.90	110.02
		40	26.0	20.3	53.25	111.03
		45	20.2	15.8	57.08	112.93
		50	17.7	13.6	62.38	117.03
1.0	0.1	30	42.8	39.7	34.61	109.02
		35	36.8	29.5	42.83	109.24
		40	23.7	19.8	45.60	112.04
		45	17.4	17.1	47.20	112.60
		50	18.3	15.9	48.02	116.71
1.0	1.0	30	34.6	31.4	40.34	112.36
		35	29.3	23.8	49.30	113.41
		40	20.2	16.2	54.28	114.72
		45	15.8	14.9	58.03	114.62
		50	14.9	13.1	63.57	120.07

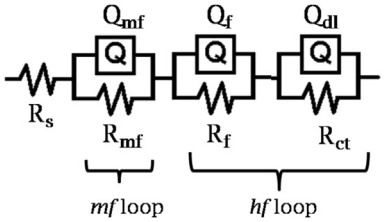

Fig. 5. Equivalent electrical circuit used for simulation of experimental impedance data points for the corrosion of ZE41 alloy in combined media of Na_2SO_4–NaCl.

the corrosion of ZE41 alloy in 0.1 M NaCl containing different concentrations of sulphate ions at 30 °C. Similar plots were obtained at all other conditions studied. The Nyquist plots presented two capacitive loops at higher and medium frequencies, followed by the beginning of an inductive loop at lower frequency region. The higher frequency (*hf*) semicircle has been attributed to charge transfer of corrosion process and oxide film effects, and the medium frequency (*mf*) semicircle to mass transport (diffusion of magnesium ions) in solid phase through the corrosion product layer. The lower frequency (*lf*) inductive loop pertains to the relaxation of surface adsorbed species like $Mg(OH)^+$ and $Mg(OH)_2$. Although impedance data interpretation for magnesium alloys remains controversial, with several other versions proposed [4,18] the current explanation has been the most adopted [6,19,36–38]. The enlargement of capacitive loops reflects reduced rate corrosion [39]. It is evident from Figs. 3 and 4 that the capacitive loops enlarge with reduced concentrations of chloride and sulphate respectively; implying that the corrosion rate diminishes with reduction in these ion concentrations. The results of EIS measurement are summarized in Table 3.

The impedance results are best understood when interpreted as equivalent circuit models simulating the electrochemical

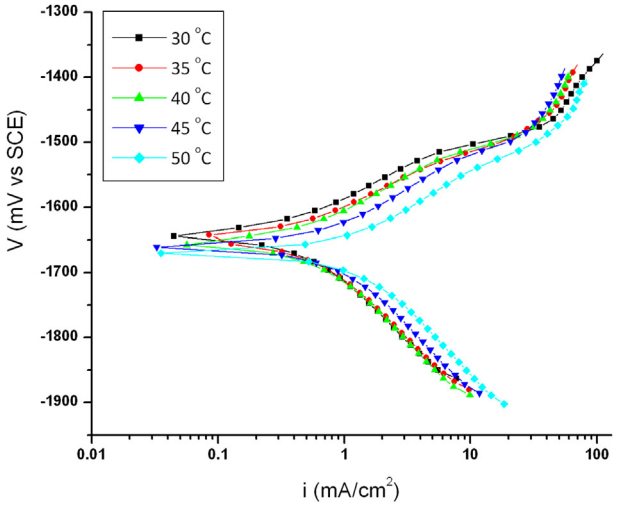

Fig. 7. Potentiodynamic polarization curves for the corrosion of ZE41 alloy in the medium 0.2 M Na_2SO_4–1.0 M NaCl at different temperatures.

behaviour of alloy–medium interface. The circuit fitment was done by ZSimpWin software of version 3.21. The impedance data points neglecting the *lf* inductive loop can be analysed using an equivalent electrical circuit (EEC) as shown in Fig. 5. The simulation of impedance data points are presented in Fig. 6. The *hf* response can be simulated by a series of two parallel resistance – constant phase element (R-CPE) networks: the charge transfer resistance (R_{ct}) in parallel with the double layer CPE (Q_{dl}) and the resistance of the surface film (R_f) in parallel with the film CPE (Q_f). The *mf* response was fitted with a parallel network of resistance (R_{dif}) and CPE (Q_{dif}) associated with diffusion [40]. The constant phase element (Q_{dl}) is substituted for the ideal capacitive element to give a more accurate fit, as only by the introduction of constant phase element the lack of homogeneity and even porosity of the electrode surface can be

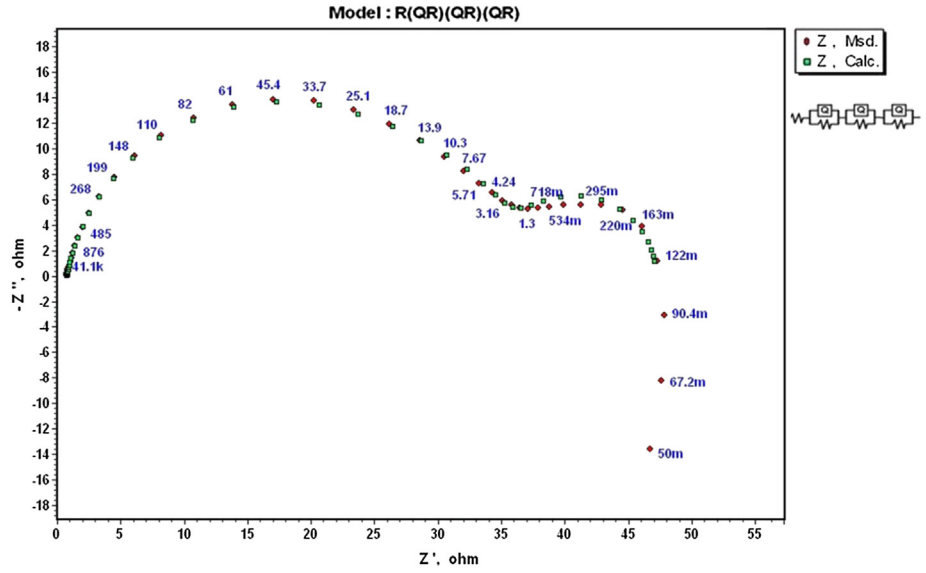

Fig. 6. The simulation of experimental impedance data points with theoretical model for the corrosion of ZE41 alloy specimen in 0.6 M Na_2SO_4 – 1.0 M NaCl at 30 °C.

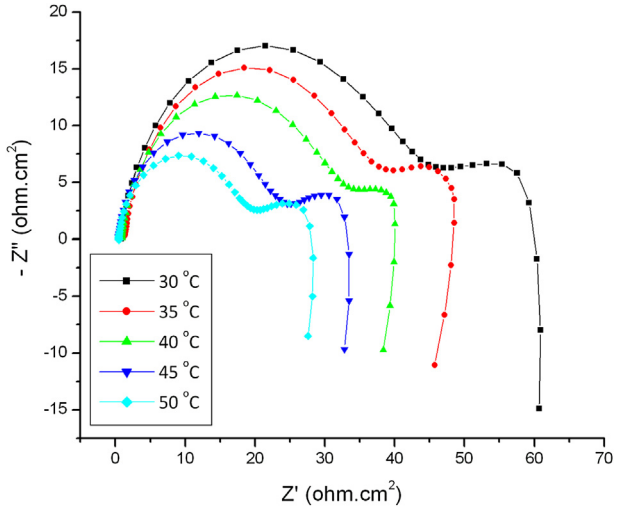

Fig. 8. Nyquist plots for the corrosion of ZE41 alloy in the medium 0.6 M Na_2SO_4–0.1 M NaCl at different temperatures.

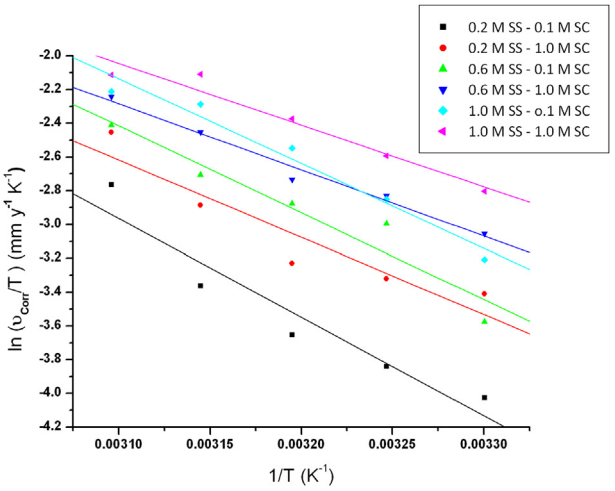

Fig. 10. Plots of $\ln(\upsilon_{corr}/T)$ vs $1/T$ for the corrosion of ZE41 alloy in the combined media of Na_2SO_4 – NaCl.

accounted. The impedance of constant phase is described by the following expression [41]:

$$Z_Q = Y_0^{-1}(j\omega)^{-n} \tag{9}$$

where Y_0 is the CPE constant, ω is the angular frequency (in rad s^{-1}), $j^2 = -1$ is the imaginary number and n is a CPE exponent which is a measure of the heterogeneity or roughness of the surface. The value of n is given by $(-1 \leq n \leq 1)$, CPE simulates an ideal capacitor when $n = 1$, an ideal inductor for $n = -1$, and an ideal resistor for $n = 0$.

The capacitance is deduced from the CPE using following expression [41]:

$$C = Y_0\left(\omega_m^n\right)^{n-1} \tag{10}$$

where, ω_m^n is the frequency at which the imaginary part of the impedance (Z'') has a maximum.

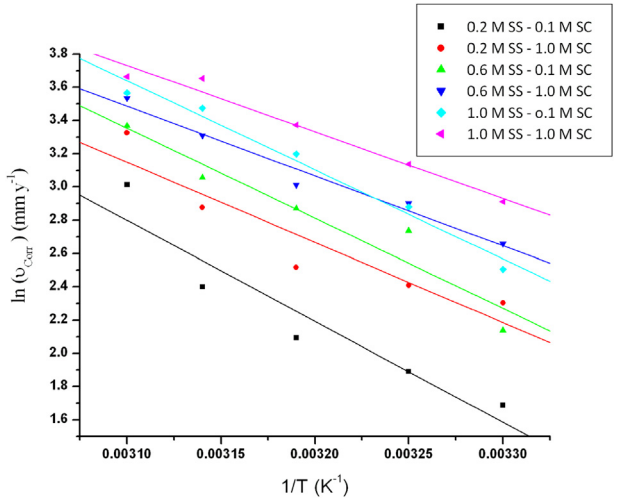

Fig. 9. Arrhenius plots for the corrosion of ZE41 alloy in the combined media of Na_2SO_4–NaCl.

The parameters deduced from impedance analysis such as R_{hf}, R_f, C_{dl}, C_f are tabulated in Table 3. It has been proposed that the collective resistance associated with the *hf* loop (R_{hf}) is inversely related to the corrosion rate [38,39]. It is evident from Table 3, that the corrosion rate increases with the increase in sulphate concentration at each chloride concentration and vice versa as indicated by the reduction in the R_{hf} values. Furthermore, in a medium with lower ionic concentration the value of R_f is higher and that of C_{dl} and C_f are lower. R_f is the measure of the protective performance of the deposited surface film and the decrease in C_{dl} and C_f can be accredited to the decrease in local dielectric constant and/or the increased thickness of the electrical double layer and the surface film, respectively, as predicted by Helmholtz model equation:

$$C_{dl} = \varepsilon/(4\pi d) \tag{11}$$

where C_{dl} is the capacitance, ε is local dielectric constant and d is thickness of double layer.

The variation of R_f and C_f together hint that at lower sulphate and chloride concentrations the formation of a thicker and more protective surface film is favoured, which offers considerable extent of protection to underlying alloy, hence the decreased rate of corrosion. The scenario is reversed at higher ionic concentrations, which can be accounted by taking into consideration the tendency of anions like sulphate and chloride to destabilize the $Mg(OH)_2$ surface film by dissolution.

3.3. Effect of temperature

The temperature as an environmental factor influencing the corrosion behaviour of ZE41 alloy was studied by measuring the corrosion rate at different temperatures in the 30 °C–50 °C range at increments of 5 °C. Fig. 7 represents the potentiodynamic polarization curves at different temperatures for the corrosion of ZE41 alloy sample in a medium of 0.2 M Na_2SO_4–1.0 M NaCl solution. Fig. 8 represents the Nyquist

Table 4
Activation parameters for the corrosion of ZE41 alloy in different concentrations of Na_2SO_4 and NaCl.

Na_2SO_4 concentration/mol dm^{-3}	NaCl concentration/mol dm^{-3}	E_a/kJ mol^{-1}	$\Delta H^{\#}$/kJ mol^{-1}	$\Delta S^{\#}$/J mol^{-1} K^{-1}
0.2	0.1	51.17	48.57	−71.65
0.2	1.0	40.59	37.99	−101.54
0.6	0.1	45.34	42.74	−85.14
0.6	1.0	35.13	32.53	−115.69
1	0.1	44.37	41.76	−85.84
1	1.0	33.016	30.41	−120.27

plots at different temperatures for the corrosion of ZE41 alloy sample in a medium of 0.6 M Na_2SO_4−0.1 M NaCl solution. Similar plots were obtained at other solution concentrations as well. With the increase in the medium temperature the polarization curves shift to the higher current density region and the capacitive loops in Nyquist plots shrink in diameter, both indicate enhanced rate of corrosion. The temperature effect is more apparent from the Tafel polarization results and EIS results at different temperatures as listed in Tables 2 and 3, respectively; it is evident that the corrosion rate increases with the increase in temperature. This has been attributed to the reduction in hydrogen evolution overpotential with the increase in temperature. The values of b_c and R_{hf} change with the varying temperature, which indicate that temperature play an influential role in the kinetics of the corrosion reactions. However the basic shape of polarization curves and Nyquist plots remain unaltered, which illustrates that temperature modifies only the rate of alloy corrosion but not the mechanism. A smaller value of C_f in combination with larger R_f is observed at lower temperatures which indicate, respectively, that the thickness and protective performance of the surface film are good at lower temperatures, in other words dissolution of $Mg(OH)_2$ surface film occurs at higher temperatures [30].

Activation energy (E_a) for the corrosion process of the alloy was calculated from the Arrhenius equation:

$$\ln(\upsilon_{\text{corr}}) = B - (E_a/RT) \tag{12}$$

where B is a constant which depends on the metal type, and R is the universal gas constant. The plot of ln (υ_{corr}) vs reciprocal of absolute temperature ($1/T$) gives a straight line and from the slope $= -E_a/R$, the activation energy values for the corrosion process were calculated. The Arrhenius plots for the corrosion of ZE41 alloy specimen are shown in Fig. 9.

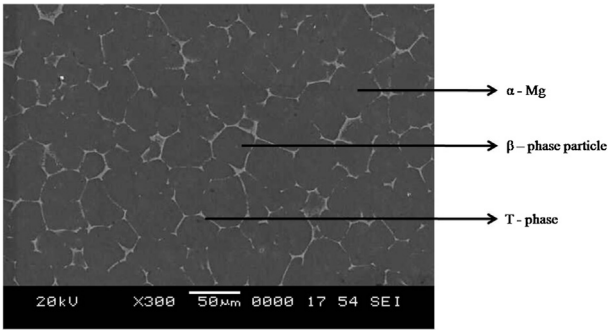

Fig. 11. SEM image of a freshly polished surface of ZE41 alloy specimen.

The enthalpy of activation ($\Delta H^{\#}$) and entropy of activation ($\Delta S^{\#}$) values for the corrosion process were calculated from the transition state theory equation:

$$\upsilon_{\text{corr}} = (RT/Nh)\exp\left(\Delta S^{\#}/R\right)\exp\left(-\Delta H^{\#}/RT\right) \tag{13}$$

where h is Planck's constant, and N is Avagadro's number and R is the ideal gas constant. A plot of $\ln(\upsilon_{corr}/T)$ vs $1/T$ gives a straight line with slope $= -\Delta H^{\#}/R$ and intercept $= \ln(R/Nh) + \Delta S^{\#}/R$. The plots of $\ln(\upsilon_{\text{corr}}/T)$ vs $1/T$ for ZE41 alloy are shown in Fig. 10.

The activation parameters calculated are listed in Table 4. The E_a value or the energy barrier for the occurrence of corrosion reaction reduces with the increased salt concentrations, which implies that the corrosion is thermodynamically more favoured in the concentrated media. The $\Delta S^{\#}$ is negative; implying the activated complex in the rate-determining step represents association rather than dissociation, indicating that a decrease in randomness takes place on going from the reactants to the activated complex [42].

3.4. Surface morphology

The surface morphology of the alloy and the effect of corrosive medium on the electrode surface were analysed using scanning electron microscopy. The SEM image of a freshly polished surface of ZE41 alloy is shown in Fig. 11. The microstructure of the alloy is evident from the image. The microstructure of ZE41 consists of the α-Mg matrix which

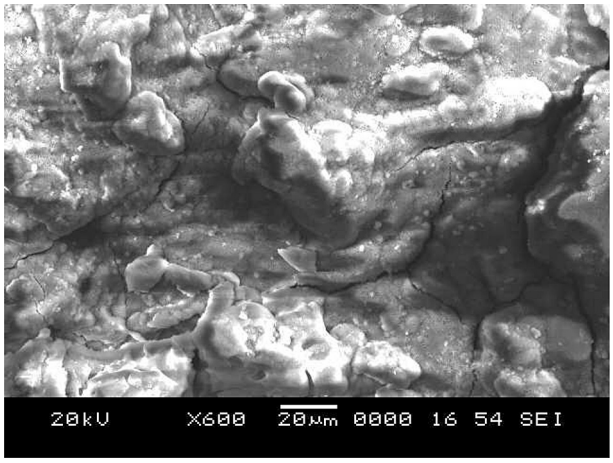

Fig. 12. SEM image of corroded surface of ZE41 alloy specimen after immersion in the medium 1.0 M Na_2SO_4 − 1.0 M NaCl for 1 h.

forms main body of the grain along with the secondary phases, consisting of randomly distributed β-phase particles and the eutectically distributed T-phase at the grain boundaries appearing as network of white mass. Fig. 12 is the SEM image of ZE41 specimen surface after immersion in a medium of 1 M Na_2SO_4 and 0.1 M NaCl for 1 h. The surface is corroded and the grain or the microstructure is hardly visible hinting a deposition occurred on the surface as a film. The surface layer appeared highly nonuniform with grooves and discontinuity in the form of breaks seen at places.

4. Conclusions

From the results of the investigation, following conclusions have been drawn:

1. The environmental factors like temperature, concentrations of sulphate and chloride have a remarkable influence on rate of corrosion of magnesium alloy ZE41.
2. The corrosion rate of magnesium alloy ZE41 increases with the increase in temperature and ionic concentration.
3. The results for electrochemical studies in combination with surface analysis confirm the formation of $Mg(OH)_2$ film on surface of the corroding specimen.
4. The $Mg(OH)_2$ surface film is partially protective due to imperfections like breaks and non-uniformity. Higher ionic concentrations and temperatures further destabilize the surface film possibly by dissolution.
5. The corrosion kinetics follows Arrhenius law.

References

[1] C. Blawert, N. Hort, K.U. Kainer, Trans. Indian Inst. Met. 57 (2004) 397−408.
[2] F.H. Froes, D. Eliezer, E. Aghion, JOM 50 (1998) 30−34.
[3] M. Gupta, N.M.L. Sharon, Magnesium Alloys and Magnesium Composites, John Wiley & Sons, NewJersy, 2011.
[4] G. Song, A. Atrens, D. StJohn, J. Nairn, Y. Li, Corros. Sci. 39 (1997) 855−875.
[5] G. Song, A. Atrens, D. StJohn, X. Wu, J. Nairn, Corros. Sci. 39 (1997) 10−11.
[6] G. Baril, N. Pebere, Corros. Sci. 43 (2001) 471−484.
[7] G. Song, D. StJohn, Corros. Sci. 46 (2004) 1381−1399.
[8] G. Song, D. StJohn, Mater. Corros. 56 (2005) 15−23.
[9] J.H. Greenblatt, J. Electrochem. Soc. 103 (1956) 539−543.
[10] M.G. Lopez, B. Natta, Corrosion 712 (2001) 5006−5015.
[11] M. Baghni, Y. Wu, J. Li, W. Zhang, Trans. Nonferrous. Met. Soc. China 14 (2004) 1−10.
[12] Y. Fan, G. Wu, C. Zhai, Mater. Sci. Eng. A 433 (2006) 208−215.
[13] S. Izumi, M. Yamasaki, Y. Kawamura, Corros. Sci. 51 (2009) 395−402.
[14] G. Song, A. Atrens, M. Dargusch, Corros. Sci. 41 (1999) 249−273.
[15] M. Sun, G. Wu, W. Wang, W. Ding, Mat. Sci. Eng. A 523 (2009) 145−151.
[16] D.K. Xu, W.N. Tang, L. Liu, Y.B. Xu, E.H. Han, J. Alloys Compd. 432 (2007) 129−134.
[17] M.C. Zhao, M. Liu, G. Song, A. Atrens, Corros. Sci. 50 (2008) 1939−1953.
[18] Y. Cheng, T. Qin, H. Wang, Z. Zhang, Trans. Nonferrous Met. Soc. China 19 (2009) 517−524.
[19] S. Mathieu, C. Rapin, J. Hazan, P. Steinmetz, Corros. Sci. 44 (2002) 2737−2756.
[20] S. Mathieu, C. Rapin, J. Steinmetz, P. Steinmetz, Corros. Sci. 45 (2003) 2741−2755.
[21] A. Pardo, S. Feliu, M.C. Merino, R. Arrabal, E. Matykina, Int. J. Corros. 2010 (2010) 8−12.
[22] N. Wang, R. Wang, C. Peng, Y. Feng, X. Zhang, Trans. Nonferrous. Met. Soc. China 20 (2010) 1936−1943.
[23] T. Rzychoń, A. Kiełbus, JAMME 17 (2006) 1−2.
[24] A.J. López, P. Rodrigo, B. Torres, J. Rams, Wear 271 (2011) 2836−2844.
[25] M.D. López, C.J. Múnez, M. Carboneras, P. Rodrigo, M.D. Escalera, E. Otero, J. Alloys Compd. 491 (2010) 131−136.
[26] M.B. Kannan, W. Dietzel, C. Blawert, A. Atrens, P. Lyon, Mater. Sci. Eng. A 480 (2008) 529−539.
[27] A.E. Coy, F. Viejo, P. Skeldon, G.E. Thompson, Corros. Sci. 52 (2010) 3896−3906.
[28] M.C. Zhao, M. Liu, G. Song, A. Atrens, Corros. Sci. 50 (2008) 3168−3178.
[29] M.G. Fontana, Corrosion Engineering, McGraw Hill, 1987.
[30] L. Wang, T. Shinohara, B. Zhang, J. Alloys Compd. 496 (2010) 500−507.
[31] R. Udhayan, D.P. Bhatt, J. Power Sources 63 (1996) 103−107.
[32] J.H. Nordlien, S. Ono, N. Masuko, K. Nisancioglu, Corros. Sci. 39 (1997) 1397−1414.
[33] G. Song, A. Atrens, Adv. Eng. Mater. 1 (1999) 11−33.
[34] G. Song, A. Atrens, Adv. Eng. Mater. 5 (2003) 837−858.
[35] G. Song, A. Atrens, Adv. Eng. Mater. 9 (2007) 177−183.
[36] H. Ardelean, I. Frateur, P. Marcus, Corros. Sci. 50 (2008) 1907−1918.
[37] E.M. Sherif, A.A. Almajid, Int. J. Electrochem. Sci. 6 (2011) 2131−2148.
[38] F. Zucchi, V. Grassi, A. Frignani, C. Monticelli, G. Trabanelli, J. Appl. Electrochem. 36 (2006) 195−204.
[39] N. Pebere, C. Riera, F. Dabosi, Electrochim. Acta 35 (1990) 555−561.
[40] S. Fletcher, J. Electrochem. Soc. 141 (1994) 1823−1826.
[41] F. Mansfeld, C.H. Tsai, H. Shih, in: R.S. Munn (Ed.), Computer Modeling in Corrosion, ASTM, Philadelphia, 1992, pp. 186−196.
[42] F. Bentiss, M. Lebrini, M. Lagrenee, Corros. Sci. 47 (2005) 2915−2931.